

Biomedical NiTi and β -Ti Alloys: from Composition, Microstructure and Thermo-Mechanics to Application

Adelaide Nespoli ¹, Francesca Passaretti ¹, László Szentmiklósi ², Boglárka Maróti ², Ernesto Placidi ³, Michele Cassetta ⁴, Rickey Y. Yada ⁵, David H. Farrar ⁶ and Kun V. Tian ^{5,6,7,*}

Citation: Nespoli, A.; Passaretti, F.; Szentmiklósi, L.; Maróti, B.; Placidi, E.; Cassetta, M.; Yada, R.Y.; Farrar, D.H.; Tian, K.V. Biomedical NiTi and β -Ti Alloys: From Composition, Microstructure and Thermo-Mechanics to Application. *Metals* **2022**, *12*, 406. <https://doi.org/10.3390/met12030406>

Academic Editors: Antonio Riveiro and Manuel Aureliano

Received: 29 December 2021

Accepted: 23 February 2022

Published: 25 February 2022

Publisher's Note: MDPI stays neutral with regard to jurisdictional claims in published maps and institutional affiliations.



Copyright: © 2022 by the authors. Licensee MDPI, Basel, Switzerland. This article is an open access article distributed under the terms and conditions of the Creative Commons Attribution (CC BY) license (<https://creativecommons.org/licenses/by/4.0/>).

- ¹ Consiglio Nazionale delle Ricerche-Istituto di Chimica della Materia Condensata e di Tecnologie per l'Energia (CNR-ICMATE), Via G. Previati 1/e, Lecco 23900, Italy; adelaide.nespoli@cnr.it (A.N.); francesca.passaretti@cnr.it (F.P.)
 - ² Budapest Neutron Center, Center for Energy Research, Budapest, 1112, Hungary; szentmiklosi.laszlo@ek-cer.hu (L.S.); maroti.boglarka@ek-cer.hu (B.M.)
 - ³ Department of Physics, Sapienza University of Rome, Piazzale Aldo Moro 5, 00185 Rome, Italy; ernesto.placidi@uniroma1.it
 - ⁴ Department of Dental and Maxillo-Facial Sciences, Sapienza University of Rome, Piazzale Aldo Moro 5, 00185 Rome, Italy; michele.cassetta@uniroma1.it
 - ⁵ Faculty of Land and Food Systems, The University of British Columbia, Vancouver, BC V6T 1Z4, Canada; r.yada@ubc.ca
 - ⁶ Department of Chemistry, McMaster University, Hamilton, ON L8S 4L8, Canada; farrard@mcmaster.ca
 - ⁷ Department of Chemical science and Pharmaceutical Technologies, Sapienza University of Rome, Piazzale Aldo Moro 5, 00185 Rome, Italy
- * Correspondence: kun.tian@uniroma1.it or tiankv@mcmaster.ca

1. Brief PGAA Fundamentals

PGAA is one of the most accurate and efficient non-destructive techniques for elemental composition, making use of the neutron-gamma-ray (n, γ) reaction, where a neutron-bombarded nucleus de-excites after neutron capture with the prompt emission of γ radiation. The energy of the γ emission is characteristic of each nucleus and the intensity of the γ peak is proportional to the number of the radiating nuclei in the sample [27–30,45].

2. Brief Neutron Diffraction Instrument Description

The details of INES have been discussed elsewhere [26] and only a brief description will be given here. It is equipped with nine detector banks, each composed of 16 ³He squashed detectors, covering an angular range 11.6–170.6° on the horizontal scattering plane. The long primary flight path ($L_0 = 22.8$ m) affords the instrument with good power for diffractive resolutions.

The differing data acquisition times for each batch were due to changes to differing samples having differing scattering intensities (due to differing elemental compositions) and thus requiring different periods of time for data acquisition to statistical certainty. Dynamic neutron flux over the measurements was also a contributing factor.

3. Three-Point Bending

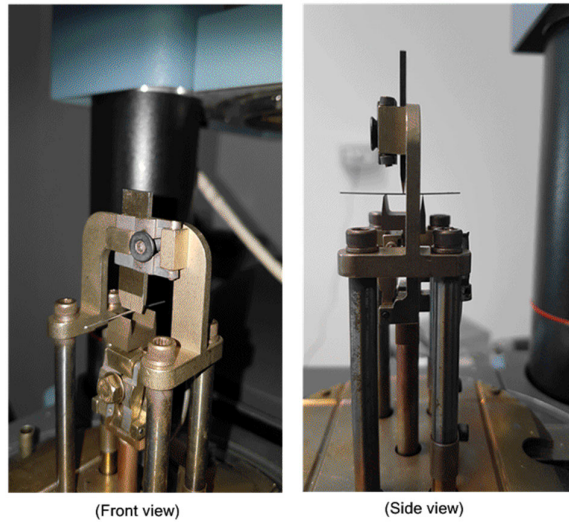


Figure S1. Photographs of the in-house-made, three-point bending test apparatus (front view) and (side view), which is composed of two 0.1 mm-radius stainless-steel fulcrums placed 10 mm apart with a centrally placed 0.1 mm-radius stainless-steel indenter above them. The apparatus is mounted on a DSC (Q100 TA Instruments, New Castle, DE, USA).

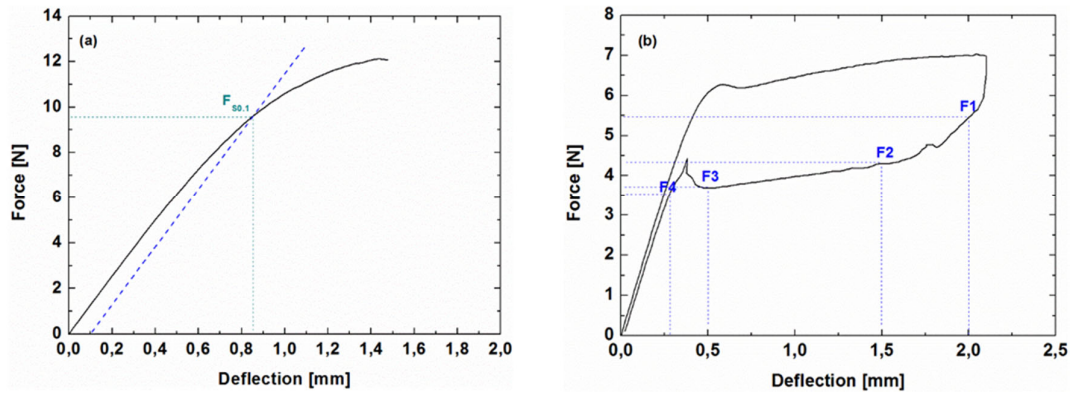


Figure S2. Representation of the force-deflection plots of the 3-point bending test on (a) β -Ti and (b) NiTi wires. The forces considered are marked.

4. Turkey Post-Hoc Test

Table S1. Tukey post-hoc test: pairwise comparison of the dimension and surface hardness $HV_{0.2}$ amongst the samples.

Pairwise comparison		Absolute difference of means					
Sample1	Sample2	height		width		$HV_{0.2}$	
β -Ti_Azdent	β -Ti_Ormco	0.0177	**	0.0008	*	0.608	*
β -Ti_Azdent	NiTi_Vis Plus	0.0165	**	0.0133	**	17.94	**
β -Ti_Azdent	NiTi_Azdent	0.0138	**	0.0128	**	43.255	**
β -Ti_Ormco	NiTi_Vis Plus	0.0012	*	0.0125	**	18.548	**
β -Ti_Ormco	NiTi_Azdent	0.0038	*	0.012	**	43.863	**
NiTi_Vis Plus	NiTi_Azdent	0.0027	*	0.0005	*	25.315	**

* not significant; ** significant at $\alpha = 0.05$.

5. DSC Heat Flow Plots

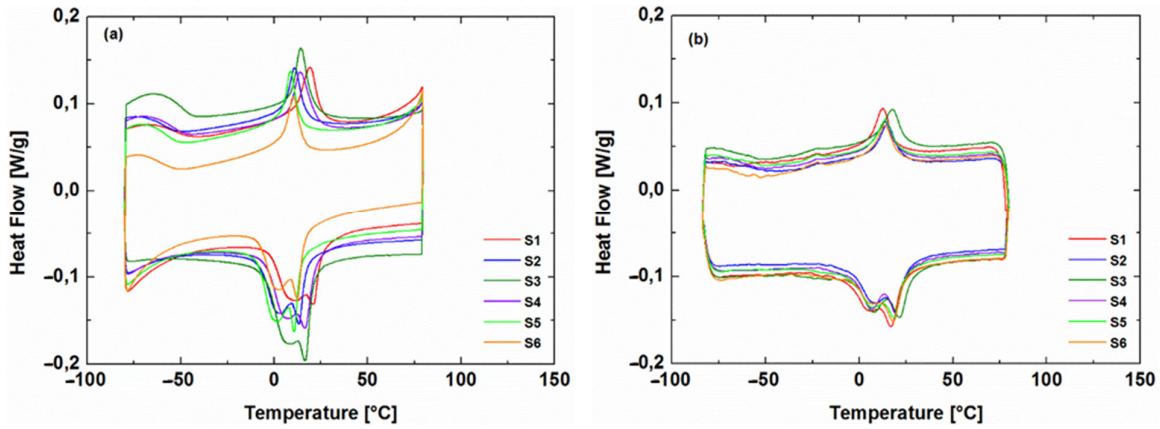


Figure S3 DSC heat flow plot of all six as-received specimens of (a) NiTi_Vis Plus and of (b) NiTi_Azdent. Specimen numbers are represented as S1–S6.

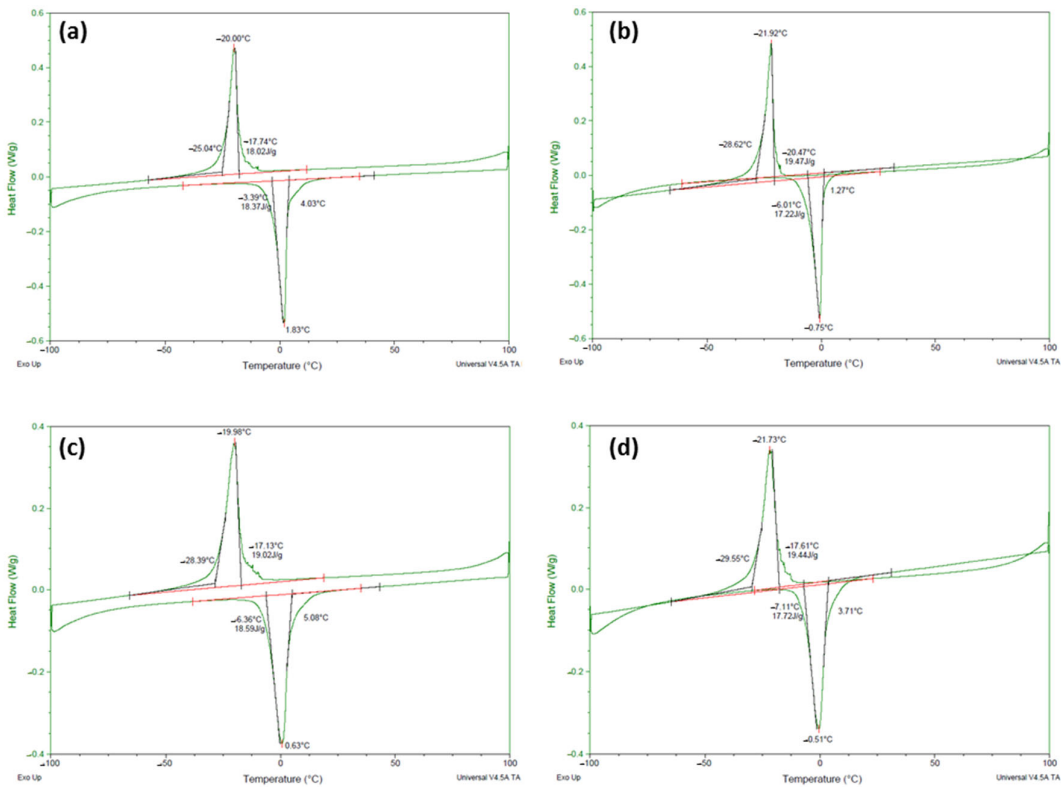


Figure S4. Heat flow plots of solubilized (a,b) NiTi_Vis Plus and (c,d) NiTi_Azdent specimens.

6. EDX Semi-Quantitative Elemental Composition Result

Table S2. Semi-quantitative elemental composition as wt.% determined by EDX.

Alloy	Brand	Ni	Ti	Mo	Zr	Sn	C
NiTi	Vis Plus	53.97	43.53	—	—	—	2.5
	Azdent	53.48	42.93	—	—	—	3.1
β-Ti	Ormco	—	75.6	11.82	5.67	4.83	—
	Azdent	—	79.49	10.89	4.84	4.78	—

7. Pearson Correlation Test Results

Table S3. Pearson correlation test results on pairs of $\Delta=T_{\text{test}}-A_f$ and bending forces F_1 – F_4 as well as force-deflection rate for NiTi products, with calculated coefficient r and p values.

Brand	Specimen	$\Delta=T_{\text{test}}-A_f$ (°C)	F_1 (N)	F_2 (N)	F_3 (N)	F_4 (N)	Force-deflection rate (N/mm)
Vis Plus	S1	10.5	4.935	3.857	3.233	3.207	13.7
	S2	19.3	5.531	4.441	3.834	3.75	15.55
	S3	15.8	4.63	3.456	2.971	3.17	13.24
	S4	14.4	4.781	3.69	3.087	3.213	14.84
	S5	22	5.466	4.314	3.708	3.758	15.17
	S6	20.1	5.624	4.437	3.871	3.714	16.72
	<i>r</i> value		0.756	0.705	0.753	0.878	0.685
	<i>p</i> value		0.081*	0.117	0.083*	0.021*	0.132
Azdent	S1	12.9	5.39551	4.23	3.56	3.49	13.41
	S2	9.8	5.5	4.24	3.41	3.2	12.89
	S3	8	5.61	4.25	3.63	3.13	12.99
	S4	10.5	5.62	4.52	3.84	3.73	14.05
	S5	10.8	5.44	4.244	3.545	3.44	13.59
	S6	11.5	5.58	4.26	3.62	3.48	13.36
	<i>r</i> value		−0.617	−0.057	−0.030	0.623	0.413
	<i>p</i> value		0.192	0.925	0.955	0.186	0.416

* Significant at $p < 0.10$.